Journal of Advanced Research in Applied Sciences and Engineering Technology

Journal homepage:
https://semarakilmu.com.my/journals/index.php/applied_sciences_eng_tech/index
ISSN: 2462-1943

A Comparative Study of Effect of Bipolar Plate Materials on Contact Resistance and Heat Transfer in a PEMFC Stack

Atifi Adil[1,*], Balli Lahcen[2], Hlimi Mohamed[2], El Bikri Khalid[1], Hamri Bachir[3]

[1] Engineering and Health Sciences and Technologies Research, M2SM, ENSAM, Mohammed V University, Rabat, Morocco
[2] Engineering Sciences and Applications Laboratory (LSIA), National School of Applied Sciences (ENSAH), Abdelmalek Essaadi University, Tetouan, Morocco
[3] Research Team Quality, Maintenance Safety QSM, Mechanical Engineering Department, Mohammadia School of Engineers, Mohammed V University, Rabat, Morocco

ARTICLE INFO

Article history:
Received 3 May 2023
Received in revised form 10 August 2023
Accepted 18 August 2023
Available online 4 September 2023

Keywords:
Bipolar plate; contact resistance; gas diffusion layers; PFMFC; heat transfer

ABSTRACT

In this paper, a comparative study based on Finite Element Method has been established in order to investigate the effect of bipolar plate materials on stress and temperature distribution in a proton exchange membrane fuel cell stack under functioning conditions. The analysis is conducted for three bipolar plate materials: Graphite BP, stamped uncoated stainless steel SS316L, and stamped Niobium coated SS316L. ICR (Interfacial contact resistance) between GDL and BP has been measured for each BP material. The effect of current densities and clamping force on contact resistance under real operating conditions have been estimated at different cell locations in the cell stack. The results show that contact resistance GDL/BP and GDL stress depend on the location of the cell in the stack especially in case of graphite BP and corroded SS316L BP. While, the Nb coated SS316L BP allows for a neglected temperature gradient between the components of the cell stack.

1. Introduction

The PEMFC stacks are composed of multiple protons exchange membranes, gas diffusion layers (GDL), catalyst layers, gaskets, and bipolar plates. The latter is one of the most important components of a fuel cell stack comprising more than 40% of the stack cost and about 80% of the total weight [1,2]. Composite graphite and graphite present low interfacial contact resistance, excellent thermos-electrical conductivity, excellent corrosion resistance, and high chemical stability [3-5]. However, poor mechanical properties and high fabrication costs are the main challenges in fuel cell development. Metallic BPs have attracted the attention of several researchers, especially in the field of transport [6]. Therefore, metal BPs with higher thermomechanical resistance, gas impermeability, and shock resistance are seen as alternative materials for the bipolar plate. In addition, thinner metallic BP can be bent easily according to the desired shape with lower manufacturing costs [7].

* *Corresponding author.*
E-mail address: adilatifi@research.emi.ac.ma

https://doi.org/10.37934/araset.32.1.343358

Several metals and alloys can be used in the manufacture of bipolar plates including stainless steel, Nickel alloys, Copper alloys, Aluminum alloys, and Titanium alloys [8]. However, the formation of a thin oxide layer on the surface of metallic BP causes an increase in the ICR between the BPs and the GDL, especially on the cathode side. Also, it allows for a drop in energy efficiency and decreases the lifetime of the sensitive elements of the cell [9-11]. Therefore, a release of poisonous metal ions can contaminate the catalyst and the membrane in both acidic and humid operating environments [12-14]. On the other hand, the optimization of the chemical composition of the metal alloys chosen for the bipolar plates may lead to not adopting the metal coating techniques [13,15,16]. In this context, optimizing the chemical composition of Chrome carbide and coating BP received more attention as an alternative way to increase the lifetime of PEMFC [14,17,18]. However, in the medium term of operation, the highly corrosive environment promotes the dissolution of the metal ions, which can contaminate the membrane and catalyst layers of the PEMFC stacks [14-18]. In comparison with other BP materials, commercial pure Niobium could be, used as an alternative material for BP, because it has a high resistance to corrosion and high chemical stability [18]. Several researchers have shown that Niobium exhibits sufficient long-term corrosion resistance in various sulfuric acid media with excellent physical properties that meet the conditions of research and development in the fields of bipolar plates for the PEMFC bipolar plate application [19,20]. Also, Nb presented lower contact resistance and neglected weight loss in the sulfuric acid environment [21-23]. The quantification of temperature generation due to the interfacial contact resistance between BP and GDL represents a major parameter for the bipolar plate's qualification and an important factor in choosing the cooling system and subsequently improving the performance and lifetime of the fuel cell stack. A strong relationship between contact resistance and assembly pressure has been found [24-26]. Several studies regarding the impact of the functioning conditions on contact resistance on PFMFC performance have been published in the case of a single cell [14,27-30]. However, the effect of cell location in the stack has received less attention. Also, most of these studies assume that ICR is constant to find correlations between clamping force and ICR. The objective of this study is to simulate both stress and temperature distribution in a PEMFC stack using two plate materials. Hence, a bi-dimensional FEM model will then be developed using Comsol Multiphysics. The proposed approach consists in solving the coupled equations of the three modules (Heat transfer, Joule heating, and mechanical structural model with thermal expansions). The boundary conditions take into account the measured ICR between BP and GDL. Table 1 below shows the DOE targets for BP performance.

Table 1
DOE targets for BP performance [31]

Characteristics	Units	2025 DOE Target
Flexural strength	Mpa	≥40
Corrosion, anode	μAcm^{-2}	<1 and no active peak
Corrosion, cathode	μAcm^{-2}	<1
Lifespan	hours	8000
Plate weight	Kg/KW	0.18
H2 Permeability	$cm^3/sec.\ Cm^2$	$2x10^{-6}$
Areal specific resistance	Ωcm^2	<0.01
Electrical conductivity	Scm-1	≥100

2. Modeling and Assumptions

2.1 Model Geometry of PEMFC Fuel Cell Side

Figure 1 describes the chosen computational domain as a PEMFC stack that contains three elements: The membrane, end plates, BP, and GDE. The geometric domain of the model is limited funds through the symmetry and the periodicity of the fuel cell stack components. According to Figure 2, PEMFC stack consists of three cells using graphite BP. While Figure 3 consists of two cells with stamped coated stainless steel bipolar plate. This is a bi-dimensional model using the FEM method under commercial software COMSOL Multiphysics's using a mechanical structural module, heat transfer module, and joule heating module. Contact resistance has been measured using Wang's approach for each bipolar plate material [34]. The assumptions adopted in our model are as follows: (1) Constant thermal conductivity (2) isotropic and homogeneous gas diffusers layers, BP, and membrane; (3) Neglected Ohmic Joule heating in the GDE and BP (4) Constant Joule heating related to the protonic transport through the membrane.

In the metallic BP (Figure 3), modeling of PEMFC Stack was limited by two cells. The cell number of the metal plates has no clear influence on the temperature distribution in the cell compared to that of graphite. This is due to the high thermal conductivity of steel compared to graphite as well as the bulk. Indeed, the thickness of the metal plates is very thin compared to the graphite plates.

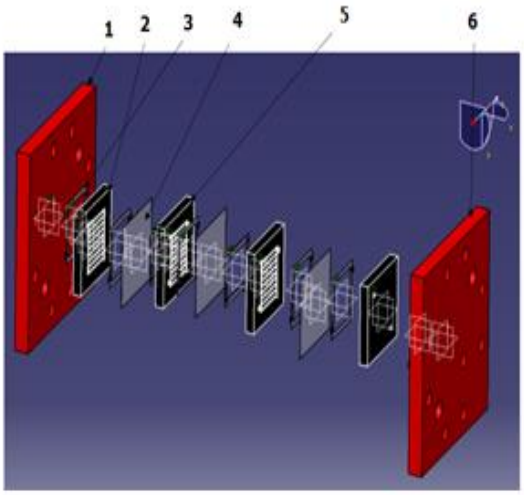

Fig. 1. Design of PFMFC stack formed by 3 cells

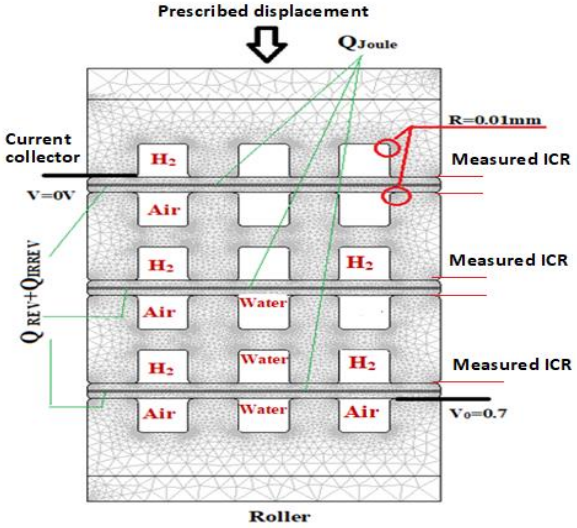

Fig. 2. Computational domain of a PEMFC Stack

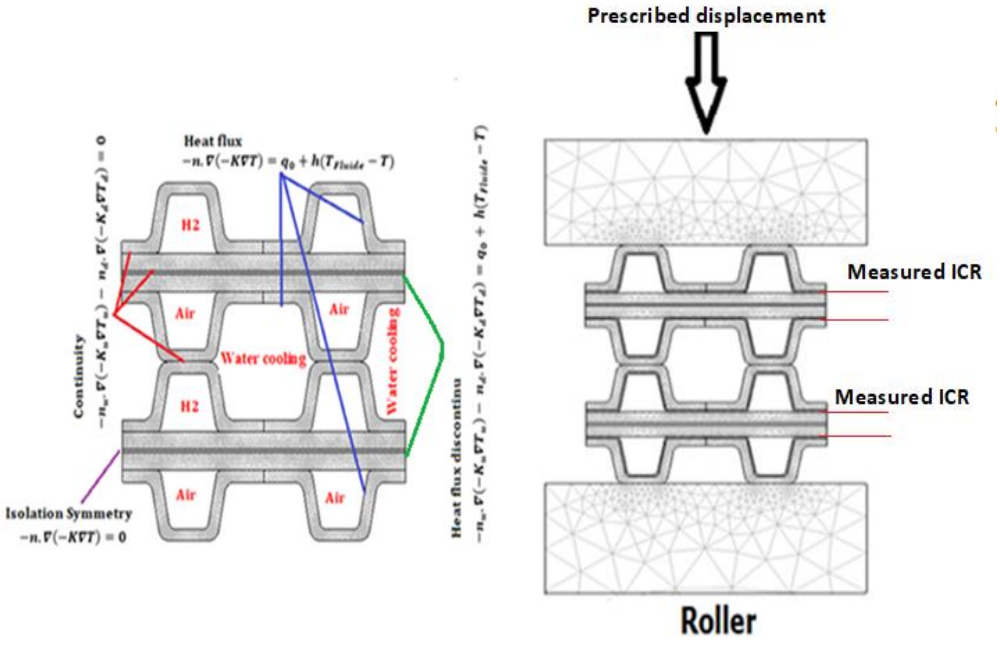

(a) (b)

Fig. 3. Computational domain of PEMFC stack formed by two cells with stamped metallic BP (a) Uncoated SS316L with heat transfer boundary conditions (b) Coated Niobium SS316L

In case of a trapezoidal canalization, Figure 4 shows the cross-sectional area Ac and the hydraulic diameter D_h are given as follow [32]:

$$D_h = \frac{a+c}{2b+a+c} \qquad S_c = \frac{a+c}{2}h \tag{1}$$

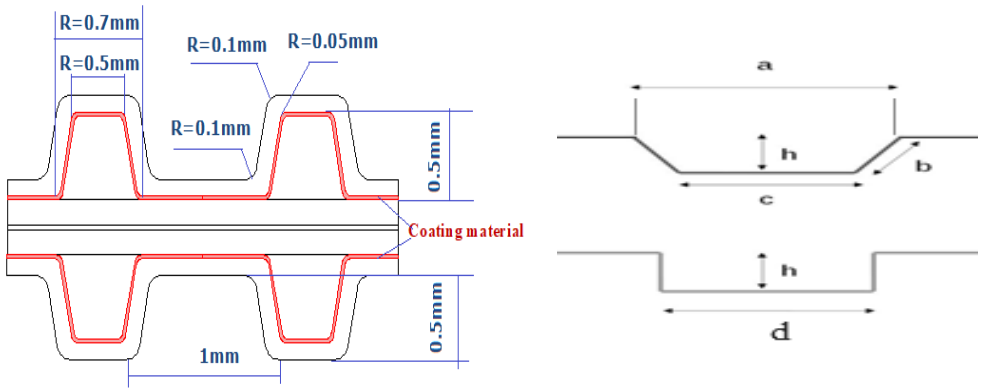

Fig. 4. Geometrical parameters of coated metallic BP

2.1.1 Heat transfer model

Contact resistance is quantified as follows:

$$Q_{c.} = (R_{BP/GDE}).i^2 \tag{2}$$

Applying Ohm's law is a way to estimate the ICR of uncoated SS316L, Nb-coated SS316L, corroded SS316L and graphite bipolar plates. According to Figure 5 and Figure 6, the specimen was placed

between two gas diffusion layers (GDL) :(TGP-H-90). To calculate the total resistance. A current of 1A was applied through two copper plates.

To measure contact resistance under actual cell operating conditions. The GDLs used in the test were previously moistened by water vapor (RH_{air}=90% GDL above and RH_{air}=30% GDL below) under a pressure of 2Mpa.

The ICR between GDL and BP material can be written as follow [33]:

$$R_{GDL/BP}=0.5(RT1-RT2) \quad (3)$$

The results show that ICR between BP and GDL are 135mΩ.cm^2, 5mΩ.cm^2 and 3mΩ.cm^2 respectively in case of Uncoated SS316 with passive film, graphite, and Nb coated SS316.

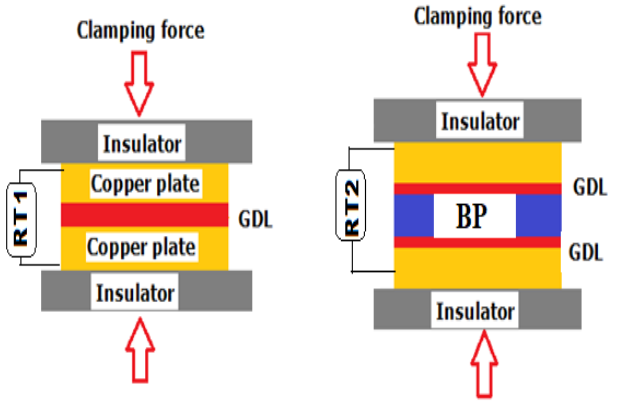

Fig. 5. The arrangement schematic of total resistances

Fig. 6. The experiment setup for ICR measurement

The general heat transfer is adopted to joule model source in the membrane:

$$\nabla.(-k\nabla T) = Q\text{-}\rho.c_p.u.\nabla T \quad (4)$$

where u=0; and Q: heat source (w/m^3).
The ohmic heat source due to the charges transport in the membrane is given as follows:

$$Q_{.} = (R_{H+})\times i^2$$

The protonic resistance in the membrane is determined by:

$$R_{H+}=\int_0^{Lm}\frac{dx}{\sigma(x)} \quad (5)$$

where the protonic conductivity can be calculated as follow [34]:

$$\sigma = (0.5139\lambda - 0.326).10^{-2}\exp[1268(\frac{1}{303}-\frac{1}{T})] \text{ (S/m)} \quad (6)$$

where;
L_m is the membrane thickness.

2.1.2 Joule heating

Electrochemical reactions and ohmic heating produce heat by the electronic current. Thus, the thermal source term in each region is

$$-\nabla.(\sigma\nabla V) = S_a.i_a$$
$$-\nabla.(\sigma\nabla V) = S_a.i_c \quad (7)$$

V is the electric potential (V); σ: is the electric conductivity (S/m); S_a is the specific surface (1e7/m)

In the catalyst layers, Butler–Volmer equations allow calculating the current density distribution due to the electrochemical reactions [35]:

$$i_a = i_{0,H2}[\exp\left(\frac{-\alpha_a n_a F\eta_a}{RT}\right) - \exp\left(\frac{(1-\alpha_a)n_a F\eta_a}{RT}\right)$$
$$i_c = i_{0,O2}[\exp\left(\frac{-\alpha_c n_c F\eta_c}{RT}\right) - \exp\left(\frac{(1-\alpha_c)n_c F\eta_c}{RT}\right) \quad (8)$$

where;
i_0: Current density at overvoltage η=0
at the equilibre $V = Eeq$, $i_{0,H2} = i_{0,O2} = i_0$
For the anode $\eta_a = E_a - E_q > 0$; for the cathode reaction $\eta_c = E_c - E_q$ <0 [36].

2.1.3 Mechanical structural model with thermal expansion

The Nafion membrane N112 is used in our model. Using the hygro-thermo-elasticity theory. The total strain tensor in the membrane is determined using the following expression [36,37]:

$$\varepsilon_{ij} = \varepsilon_{ij}^M + \varepsilon_{ij}^T + \varepsilon_{ij}^S \quad (9)$$

The thermal strains can be calculated as a function of the thermal expansion coefficient, and the temperature [36]:

$$\varepsilon_{ij}^T = \alpha(T - T_0)\delta_{ij} \quad (10)$$

with $\delta_{ij} = \begin{cases} 1\ si\ i = j \\ 0\ si\ i \neq j \end{cases}$

In the case of GDE and BP the effect of stress due to moisture is neglected. Plane stress components, σ_{yy} and . σ_{xx} we focus on the calculation of in-plane component stress tensor [38,39]:

$$\sigma_{xx}=\frac{E\nu}{(1+\nu)(1-2\nu)}\left(\varepsilon_{xx}+\varepsilon_{yy}+\varepsilon_{zz}\right)+\frac{E}{(1+\nu)}\varepsilon_{xx}-\frac{E}{3(1-2\nu)}(\alpha\Delta T)$$
$$\sigma_{yy}=\frac{E\nu}{(1+\nu)(1-2\nu)}\left(\varepsilon_{xx}+\varepsilon_{yy}+\varepsilon_{zz}\right)+\frac{E}{(1+\nu)}\varepsilon_{yy}-\frac{E}{3(1-2\nu)}(\alpha\Delta T) \quad (11)$$

Table 2 below outline the physical properties of PEMFC stack materials.

Table 2
Physical properties of PEMFC stack materials

Properties	Unit	Value
Ambient temperature	T_{air}	30°C
Catholic transfer coefficient	α	1
Cooling temperature	T_{water}	60-80°C
Current density	$i(A/m^2)$	5e3-15e3
The density of Graphite, Nafion, GDE, Niobium, SS316L	$\rho(Kg/m^3)$	1800,2000,450,7190,8000
Electric conductivity of Graphite, GDE, Niobium and SS316L	$\sigma(\frac{S}{m})$	1500,1500,6.93e6,1.73e3
Gas mixture velocity (m/s)	V(m/s)	2
Anodic Current Exchange density	$i_{0,a}$ (A/cm^2)	1e-8
Cathodic Current Exchange density	$i_{0,c}$ (A/cm^2)	1e-3
Faraday constant, F	F(C/mole)	96487
Hydrogen heat transfer coefficient of hydrogen	$h_{H2}(W/K.m^2)$	680
Water vapor heat transfer coefficient	h_{H2O}	2204
Air transfer coefficient	h_{Air}	99
Heat source	$Q(W/m^3)$	-
Universal gas constant	R (J/mol.L)	8.314
Inward heat flux	q_0 (W/m^2)	-
Membrane thickness, GDE thickness	$L_m(m)$	50µm, 200µm
Poisson's ration of Graphite, GDE,Nafion, Niobium, SS316L	v	0.25,0.25,0.3,0.25,0.27
Thermal conductivity of Graphite, GDE, Nafion, Niobium and SS316L	K	95,0.3,0.259,53.7,16.3
Thermal expansion coeff of Graphite, GDE, Nafion,Niobium and SS316L	α (1/K)	5e-6, -0.8e-6, 121e-6, 6e-6, 15.9e-5
Specific heat capacity ofGraphite, GDE, Nafion, Niobium and SS316L	$Cpn(J.Kg.K^{-1})$	750,500,1050,265,500
Specific surface	Sa	1e7/m
Young modulus of graphite BP, GDL, Membrane, Niobium, SS316L	MPa	10000,1000, 146,105e3,193e3
Water content in the membrane	λ	14
Cronicker symbol	δ_{ij}	

3. Results and Discussion

3.1 Effect of Graphite Bipolar Plate on Voltage and Temperature Distribution

In order to obtain high or medium power for most applications a multitude of single cells must be connected to form a PEM fuel cell stack [40,41]. The electrical circuit is closed between the first anode and the last cathode of the fuel cell stack. The cells must be connected in series to obtain a higher total voltage [40]. Figure 7 simulates electric potential distribution under an imposed displacement of e=60µm. For each cathodic side, an imposed potential of 0.7 has been considered as a boundary condition. For each GDL/BP contact, an imposed measured joule heating due to the ICR has been considered. The results show a maximum potential of 2.1Volt between the first anode, and the last cathodic fuel cell stack. The arrows represent the total current density circulation.

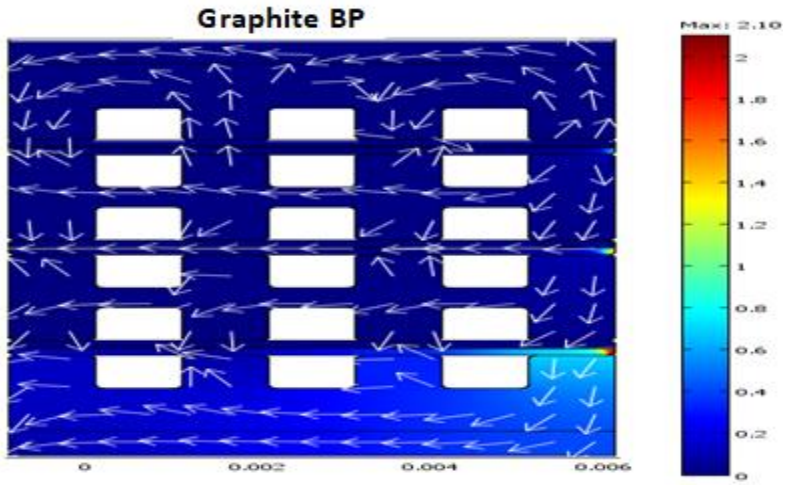

Fig. 7. Potential distribution in the PFMFC stack in case of graphite BP, the arrows show the total current density-surface

On the other hand, it is well known that PEMFCs operate at a lower temperature than other fuel cell types, less than 100°C, typically in the range of 70°C to 85°C. Stacking several fuel cells with heterogeneous elements produces larger heat generations including Joule heating, irreversible heat, and entropic heat of reactions [40-43]. The heat produced leads to a serious breakdown of the membrane since the latter has a glass transition temperature Tg ranging between 80°C and 120°C [44]. The temperature must be removed using a water-cooling system, especially in the case of PEMFCs larger than 10KW. Figure 8(a) and Figure 8(b) Show the temperature distribution in the fuel cell stack for two different levels of current density 1.5A/cm^2 and 0.5A/cm^2. Despite the existence of a water-cooling circuit at 70°C. An increase from medium to high current density allows for an increase in maximum temperature of 2° C. The temperature in the cathodic side is higher than that of the anodic side of each cell, particularly for high current density (1.5A/cm2) under the channel.

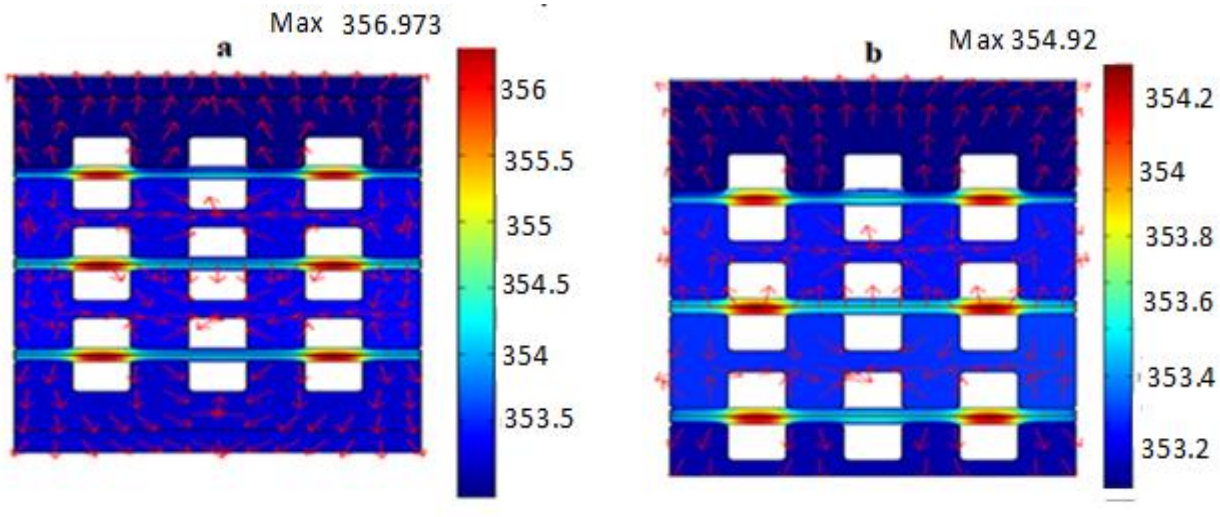

(a) (b)

Fig. 8. Temperature distribution in the stack in case of graphite BP at (a) i=1.5A/cm^2 (b) i=0.5/cm^2 (the arrow shows the total heat flux)

Another source of heat that due to the contact pressure between the porous structure of the gas diffusion layers and the bipolar plate surface roughness. As the membrane and GDL are the heart and most sensitive components of the fuel cell. Too high contact pressure between BP and GDL can over-

compress both GDL and the thinner membrane deteriorating their porous structures. Several research has revealed that contact resistance between BP and GDL constitutes an important part of Joule heating resistance. Figure 9 shows that the contact pressure is not uniform. It depends on the location of the cell. Therefore, the farther the cell is from the clamping force, the lower the contact pressure and therefore the higher the contact resistance. Therefore, the Joule effect due to the ICR is added to that of the proton resistance. However, the closer the cell is to the clamping force, the lower the contact resistance. Hence, the GDL of the first cell is more deformed, and stress distributions are heterogeneous and maximal on the rib side.

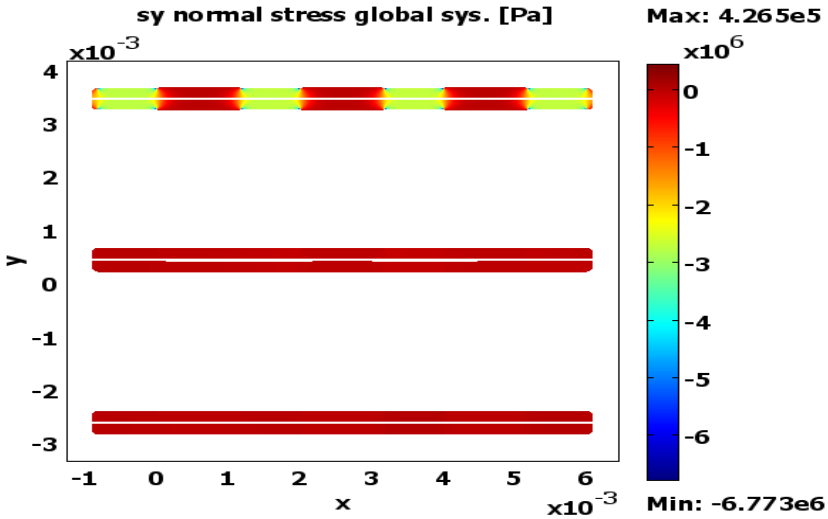

Fig. 9. = Stress distribution in each cell of the stack under an imposed displacement of e=60µm; T_{cool}=80°C and I=1.5A/cm^2

Several researchers have studied contact resistance as a function of the clamping force. However, few among them have studied ICR regarding functioning conditions like temperature and current density. In addition, the models consider constant ICR and do not depend on cell location in the stack, because the functioning conditions of fuel cell stacks are not the same in comparison with that of a single PEM fuel cell. The effect of current density on the stress distribution has been simulated in the most deformed GDL in the cell stack. Figure 10 shows that the contact pressure is maximal and located in the GDL/BP interface where there is the maximum stress concentration. However, this contact pressure remains uniform in the rib approximately 2.5e6Pa. The results show that an increase in current density from 0.5A/cm^2 to 1.5A/cm^2 leads to an increase in maximum contact pressure from 5.53e6Pa to 6.662e6Pa.

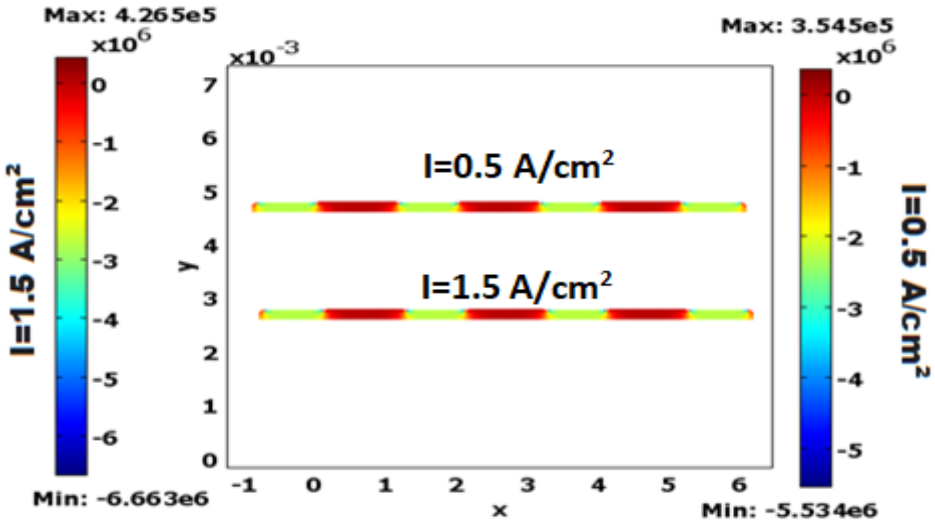

Fig. 10. Contact pressure distribution in the anodic cell1 under two current densities under an imposed displacement of e=60µm

The quantification of temperature generation represents a key factor for optimizing bipolar plate materials and consequently, will improve the efficiency and lifetime of a PEMFC stack. Therefore, the numerical resolution of coupling general heat transfer and mechanical structural equations allows for estimating the effect of the cell location in the stack on interfacial contact resistance. Hence, in the case of a graphite BP. Figure 11 shows the profile of temperature in interfacial BP/ GDL, as a result, the maximum contact pressure is located at the cathodic side of the first cell. The variation of the imposed displacement in the end plate has been investigated for three cases (e=10 µm, e=30 µm, and e=60µm). It can be seen that a neglected increase in temperature with decreasing contact pressure on the rib side. Hence, increasing contact pressure decreases ICR. However, it over-compresses the GDL, because of increasing the effective contact area between BP and GDL.

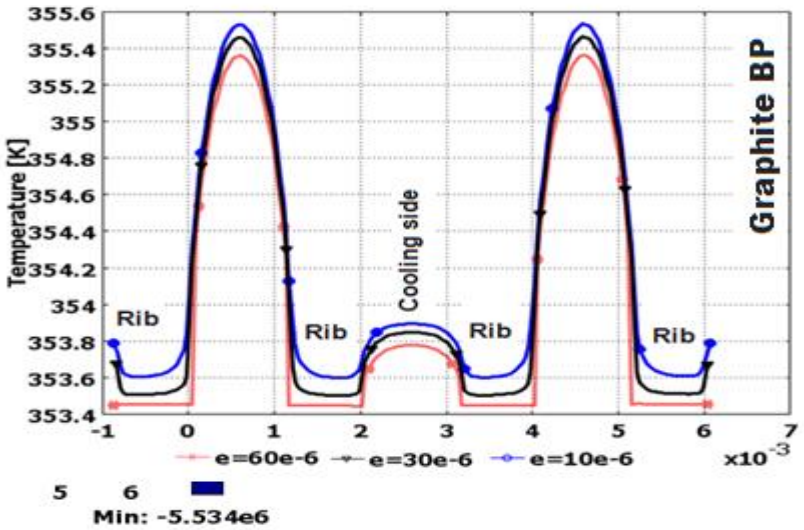

Fig. 11. Temperature profile in the contact BP/GDL under three imposed displacements

On the other hand, the Figure 12 compares the temperature profile at the GDL/BP contact for each cell in the stack. The results show that the temperature on the cathodic sides always remains higher than that of the anodic side with a small difference less than 1°C and this is thanks to the cooling circuit with a higher convective coefficient. Therefore, the contact resistance depends on the location of the cell in the stack. It is clear that as long as one moves away from the clamping pressure, the contact resistance decreases, which translates to an increased temperature in the GDL / BP, interface.

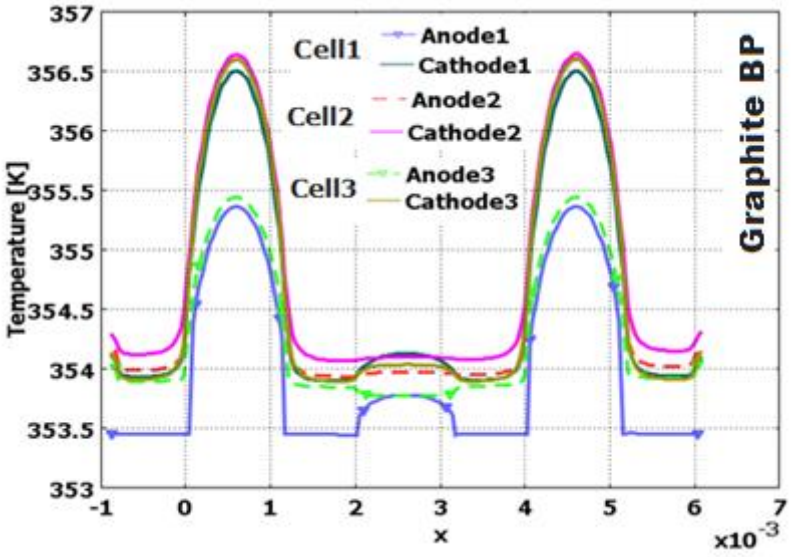

Fig. 12. Temperature profile in each cell location: e=60e-6, I=1.5A/cm^2 with temperature cooling of 70°C

3.2 Effect of the Metallic Bipolar Plate on Contact Resistance and Temperature

Figure 13(a) and Figure 13(c) compare the temperature profile at the interface GDL/BP between two fuel cell stacks in case of a medium current density of 0.5A/cm^2 and a cooling temperature of 70°C. Therefore, it can be seen that the existence of a thin oxide layer on the surface of BP allows for an increase in temperature of about 3°C. This increase in temperature due to the presence of an oxide film will become more significant in cases of high current density and depend on cell location. The temperature on the cathode side is always slightly higher than that on the anode side. This is due to the heat coming from the electrochemical reactions, which are slow on the cathode side and are strongly dependent on current density. On the other hand, low PEMFCs authorize small temperature variations and a large amount of waste heat indicating that a cooling system is necessary for optimizing fuel cell stack temperature distribution. As a temperature of 80°C constitutes the ideal operating temperature for PEMFCs, a cooling circuit of 60°C to 70°C is suitable and adopted in all applications of this technology in the event of medium and high power to evacuate the increase in temperature due to over-voltages. Figure 13(a) and Figure 13(b) show the effect of the cooling system on the temperature profiles at the GDL/BP contact in four zones of the PEMFC stack : Anode1, Cathode1, Anode2, and Cathode2. It can be seen that a cooling circuit of T=60°C makes the temperature profile more homogeneous at the level of the ribs (353K). The temperature in the channel are identical on the cathodic side as well as on the anodic side with a difference of 1°K between the first and the last cell.

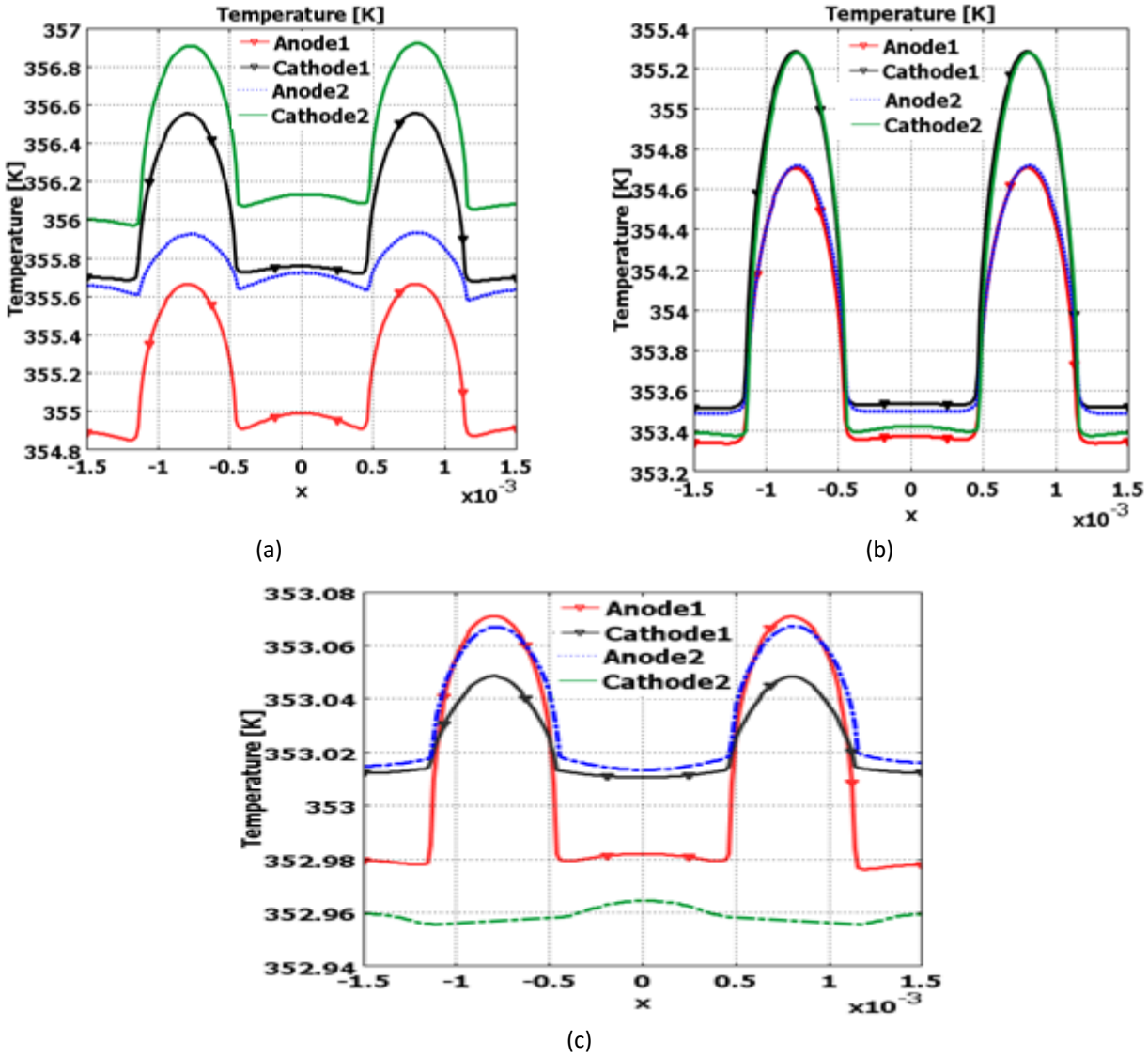

Fig. 13. Temperature profile at the GDL/BP interface in case of Metallic SS316L BP (a) Uncoated SS316L BP with passive film (T_{cool}=70°C) (b) Uncoated SS316L BP with passive film (T_{cool}=60°C) (c) Uncoated SS316L BP without passive film (T_{cool}=70°C)

On the other hand, Figure 14 shows the temperature distribution in the case of a Niobium coated SS316 BP Under a high current density of 1.5A/cm^2. It's clear that the temperature distribution is homogeneous and don't depend on cell location, which is a great advantage over other kinds of coating despite its high cost compared to Several metals and alloys including stainless steel, Nickel alloys, Copper alloys, chromium alloys, Aluminum alloys, and Titanium alloys. Therefore, a neglected temperature gradient of 0.2° C between the anodic BP of the first cell and the cathodic BP of the second cell thanks to the existence of the cooling system. It should also be noted that Nb coated SS316L makes the temperature almost identical between the channel and the rib. The trend can be explained by the large value of the thermal expansion coefficient and thermal conductivity of Nb in comparison with other coating materials, Bipolar plates. On the other hand, Figure 15(b) shows the Von Mises stress distribution in metallic SS316L Bipolar plates. It's can be observed that the stress distribution is uniform at the interface GDL/BP about 1.5e9Pa, and maximal in the corners about 2e9 Pa. In addition, coating materials must be uniform and adhere to the metal of BP to eliminate the formation of pinholes and micro-cracks, especially in corners (Figure 15(a)) where, there is maximum stress which allows acceleration of localized corrosion.

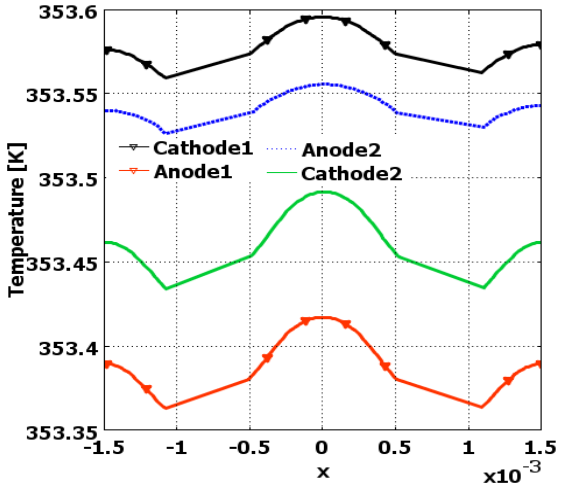

Fig. 14. Temperature profile for NB Coated SS316L bipolar plate

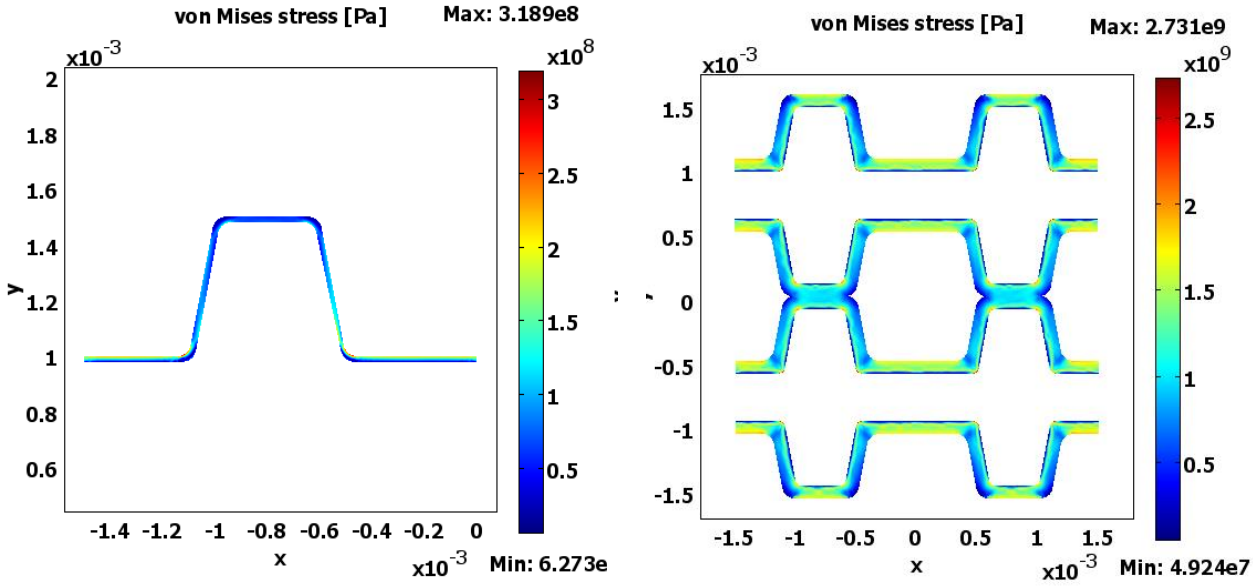

(a) (b)

Fig. 15. Stress distribution (a) In the Nb Layer (b) In the SS316L BP

4. Conclusion

A two-dimensional model using the FEM method has been established to compare the effect of cell location on stress and distribution in the cell stack. In addition, a comparative study has been established to investigate the effect of both the presence of passive film and Nb coated SS316L BP on temperature profile and ICR using a mechanical structural module, heat transfer module, and joule-heating module. The results show contact resistance depends on cell location and current density in case of graphite and corroded SS316L BP. As a result, the farther the cell is from the clamping force, the lower the contact pressure and therefore the higher the contact resistance. In addition, the results show that the temperature distribution in the case of a Niobium-coated SS316 BP allows for a neglected temperature gradient between the components of the cell stack. Furthermore, the presence of a system cooling circuit of T=60°C makes the temperature more homogeneous between the rib and the channel and not depend on the location of the cell.

Acknowledgement
This research was not funded by any grant.

References
[1] Hermann, Allen, Tapas Chaudhuri, and Priscila Spagnol. "Bipolar plates for PEM fuel cells: A review." *International journal of hydrogen Energy* 30, no. 12 (2005): 1297-1302. https://doi.org/10.1016/j.ijhydene.2005.04.016
[2] Tang, Aubrey, Louis Crisci, Leonard Bonville, and Jasna Jankovic. "An overview of bipolar plates in proton exchange membrane fuel cells." *Journal of Renewable and Sustainable Energy* 13, no. 2 (2021). https://doi.org/10.1063/5.0031447
[3] Fu, Yu, Guoqiang Lin, Ming Hou, Bo Wu, Zhigang Shao, and Baolian Yi. "Carbon-based films coated 316L stainless steel as bipolar plate for proton exchange membrane fuel cells." *International Journal of hydrogen energy* 34, no. 1 (2009): 405-409. https://doi.org/10.1016/j.ijhydene.2008.10.068
[4] Kumagai, Masanobu, Seung-Taek Myung, Shiho Kuwata, Ryo Asaishi, and Hitoshi Yashiro. "Corrosion behavior of austenitic stainless steels as a function of pH for use as bipolar plates in polymer electrolyte membrane fuel cells." *Electrochimica Acta* 53, no. 12 (2008): 4205-4212. https://doi.org/10.1016/j.electacta.2007.12.078
[5] Mehta, Viral, and Joyce Smith Cooper. "Review and analysis of PEM fuel cell design and manufacturing." *Journal of power sources* 114, no. 1 (2003): 32-53. https://doi.org/10.1016/S0378-7753(02)00542-6
[6] Hentall, Philip L., J. Barry Lakeman, Gary O. Mepsted, Paul L. Adcock, and Jon M. Moore. "New materials for polymer electrolyte membrane fuel cell current collectors." *Journal of Power Sources* 80, no. 1-2 (1999): 235-241. https://doi.org/10.1016/S0378-7753(98)00264-X
[7] Fritz, Willy. "Numerical simulation of the peculiar subsonic flow-field about the VFE-2 delta wing with rounded leading edge." *Aerospace Science and Technology* 24, no. 1 (2013): 45-55. https://doi.org/10.1016/j.ast.2012.02.006
[8] Chu, Julio. *Experimental surface pressure data obtained on 65 delta wing across Reynolds number and Mach number ranges*. Vol. 3. National Aeronautics and Space Administration, Langley Rearch Center, 1996.
[9] Lee, Shuo-Jen, Ching-Han Huang, and Yu-Pang Chen. "Investigation of PVD coating on corrosion resistance of metallic bipolar plates in PEM fuel cell." *Journal of materials processing technology* 140, no. 1-3 (2003): 688-693. https://doi.org/10.1016/S0924-0136(03)00743-X
[10] Huang, N. B., H. Yu, L. S. Xu, S. Zhan, M. Sun, and Donald W. Kirk. "Corrosion kinetics of 316L stainless steel bipolar plate with chromiumcarbide coating in simulated PEMFC cathodic environment." *Results in physics* 6 (2016): 730-736. https://doi.org/10.1016/j.rinp.2016.10.002
[11] Wang, Heli, and John A. Turner. "Ferritic stainless steels as bipolar plate material for polymer electrolyte membrane fuel cells." *Journal of Power Sources* 128, no. 2 (2004): 193-200. https://doi.org/10.1016/j.jpowsour.2003.09.075
[12] André, Johan, Laurent Antoni, Jean-Pierre Petit, Eric De Vito, and Alexandre Montani. "Electrical contact resistance between stainless steel bipolar plate and carbon felt in PEFC: A comprehensive study." *International Journal of Hydrogen Energy* 34, no. 7 (2009): 3125-3133. https://doi.org/10.1016/j.ijhydene.2009.01.089
[13] Davies, D. P., P. L. Adcock, M. Turpin, and S. J. Rowen. "Stainless steel as a bipolar plate material for solid polymer fuel cells." *Journal of power sources* 86, no. 1-2 (2000): 237-242. https://doi.org/10.1016/S0378-7753(99)00524-8
[14] Antunes, Renato A., Mara Cristina L. Oliveira, Gerhard Ett, and Volkmar Ett. "Corrosion of metal bipolar plates for PEM fuel cells: A review." *International journal of hydrogen energy* 35, no. 8 (2010): 3632-3647. https://doi.org/10.1016/j.ijhydene.2010.01.059
[15] Adcock, P., A. Kells, and C. Jackson. "EET-2008 European Ele-Drive Conference Proceedings." In *International Advanced Mobility Forum, Geneva, Switzerland*. 2008.
[16] Hornung, R., and G. Kappelt. "Bipolar plate materials development using Fe-based alloys for solid polymer fuel cells." *Journal of Power Sources* 72, no. 1 (1998): 20-21. https://doi.org/10.1016/S0378-7753(97)02774-2
[17] Wang, L., D. O. Northwood, X. Nie, J. Housden, E. Spain, A. Leyland, and A. Matthews. "Corrosion properties and contact resistance of TiN, TiAlN and CrN coatings in simulated proton exchange membrane fuel cell environments." *Journal of Power Sources* 195, no. 12 (2010): 3814-3821. https://doi.org/10.1016/j.jpowsour.2009.12.127
[18] Kim, Yu-Sung, In-Sik Lee, Jin-Young Choi, Shinhee Jun, Daeil Kim, Byung-Chul Cha, and Dae-Wook Kim. "Corrosion behavior of niobium-coated 316L stainless steels as metal bipolar plates for polymer electrolyte membrane fuel cells." *Materials* 14, no. 17 (2021): 4972. https://doi.org/10.3390/ma14174972
[19] Weil, K. Scott, Gordon Xia, Z. Gary Yang, and Jin Yong Kim. "Development of a niobium clad PEM fuel cell bipolar plate material." *International Journal of Hydrogen Energy* 32, no. 16 (2007): 3724-3733. https://doi.org/10.1016/j.ijhydene.2006.08.041

[20] Pozio, A., R. F. Silva, and A. Masci. "Corrosion study of SS430/Nb as bipolar plate materials for PEMFCs." *International Journal of Hydrogen Energy* 33, no. 20 (2008): 5697-5702. https://doi.org/10.1016/j.ijhydene.2008.05.099

[21] Kim, Ae Rhan, Mohanraj Vinothkannan, and Dong Jin Yoo. "Sulfonated fluorinated multi-block copolymer hybrid containing sulfonated (poly ether ether ketone) and graphene oxide: A ternary hybrid membrane architecture for electrolyte applications in proton exchange membrane fuel cells." *Journal of energy chemistry* 27, no. 4 (2018): 1247-1260. https://doi.org/10.1016/j.jechem.2018.02.020

[22] Kim, Yu-Sung, In-Sik Lee, Jin-Young Choi, Shinhee Jun, Daeil Kim, Byung-Chul Cha, and Dae-Wook Kim. "Corrosion behavior of niobium-coated 316L stainless steels as metal bipolar plates for polymer electrolyte membrane fuel cells." *Materials* 14, no. 17 (2021): 4972. https://doi.org/10.3390/ma14174972

[23] Kim, Ae Rhan, Chul Jin Park, Mohanraj Vinothkannan, and Dong Jin Yoo. "Sulfonated poly ether sulfone/heteropoly acid composite membranes as electrolytes for the improved power generation of proton exchange membrane fuel cells." *Composites Part B: Engineering* 155 (2018): 272-281. https://doi.org/10.1016/j.compositesb.2018.08.016

[24] Kahraman, H., I. Cevik, F. Dündar, and F. Ficici. "The corrosion resistance behaviors of metallic bipolar plates for PEMFC coated with physical vapor deposition (PVD): an experimental study." *Arabian Journal for Science and Engineering* 41, no. 5 (2016): 1961-1968. https://doi.org/10.1007/s13369-016-2058-x

[25] Forouzanmehr, Mohsen, Kazem Reza Kashyzadeh, Amirhossein Borjali, Mosayeb Jafarnode, and Mahmoud Chizari. "Effects of CrN/TiN coatings on interfacial contact resistance of stainless steel 410 bipolar plates in fuel cells." In *Energy and Sustainable Futures: Proceedings of 2nd ICESF 2020*, pp. 133-139. Cham: Springer International Publishing, 2021. https://doi.org/10.1007/978-3-030-63916-7_17

[26] Forouzanmehr, Mohsen, Kazem Reza Kashyzadeh, Amirhossein Borjali, Anastas Ivanov, Mosayeb Jafarnode, Tat-Hean Gan, Bin Wang, and Mahmoud Chizari. "Detection and analysis of corrosion and contact resistance faults of TiN and CrN coatings on 410 stainless steel as bipolar plates in PEM fuel cells." *Sensors* 22, no. 3 (2022): 750. https://doi.org/10.3390/s22030750

[27] Feng, Kai, Yao Shen, Hailin Sun, Dongan Liu, Quanzhang An, Xun Cai, and Paul K. Chu. "Conductive amorphous carbon-coated 316L stainless steel as bipolar plates in polymer electrolyte membrane fuel cells." *International journal of hydrogen energy* 34, no. 16 (2009): 6771-6777. https://doi.org/10.1016/j.ijhydene.2009.06.030

[28] Wang, L., D. O. Northwood, X. Nie, J. Housden, E. Spain, A. Leyland, and A. Matthews. "Corrosion properties and contact resistance of TiN, TiAlN and CrN coatings in simulated proton exchange membrane fuel cell environments." *Journal of Power Sources* 195, no. 12 (2010): 3814-3821. https://doi.org/10.1016/j.jpowsour.2009.12.127

[29] Bi, Feifei, Peiyun Yi, Tao Zhou, Linfa Peng, and Xinmin Lai. "Effects of Al incorporation on the interfacial conductivity and corrosion resistance of CrN film on SS316L as bipolar plates for proton exchange membrane fuel cells." *International Journal of Hydrogen Energy* 40, no. 31 (2015): 9790-9802. https://doi.org/10.1016/j.ijhydene.2015.06.012

[30] Hedayati, Ali, Saeed Asghari, Amir Hosein Alinoori, Morteza Koosha, and Esa Vuorinen. "Effects of coating thickness on corrosion and contact resistance behavior of TiN coated AISI 316L as bipolar plates for PEMFC." *Iranian Journal of Hydrogen & Fuel Cell* 3, no. 2 (2016): 137-149.

[31] Drive, U. "Fuel cell technical team roadmap." *New York: US Drive Partnership* (2013): 1-26.

[32] Reimer, Uwe, Dieter Froning, Gert Nelissen, Leonard FJM Raymakers, Shidong Zhang, Steven B. Beale, and Werner Lehnert. "An engineering toolbox for the evaluation of metallic flow field plates." *ChemEngineering* 3, no. 4 (2019): 85. https://doi.org/10.3390/chemengineering3040085

[33] Wang, Heli, Mary Ann Sweikart, and John A. Turner. "Stainless steel as bipolar plate material for polymer electrolyte membrane fuel cells." *Journal of Power Sources* 115, no. 2 (2003): 243-251. https://doi.org/10.1016/S0378-7753(03)00023-5

[34] Springer, Thomas E., T. A. Zawodzinski, and Shimshon Gottesfeld. "Polymer electrolyte fuel cell model." *Journal of the electrochemical society* 138, no. 8 (1991): 2334. https://doi.org/10.1149/1.2085971

[35] Larminie, James, Andrew Dicks, and Maurice S. McDonald. *Fuel cell systems explained*. Vol. 2. Chichester, UK: J. Wiley, 2003. https://doi.org/10.1002/9781118878330

[36] Tang, Yaliang, Anette M. Karlsson, Michael H. Santare, Michael Gilbert, Simon Cleghorn, and William B. Johnson. "An experimental investigation of humidity and temperature effects on the mechanical properties of perfluorosulfonic acid membrane." *Materials Science and Engineering: A* 425, no. 1-2 (2006): 297-304. https://doi.org/10.1016/j.msea.2006.03.055

[37] Al-Baghdadi, Maher AR Sadiq. "A parametric study of assembly pressure, thermal expansion, and membrane swelling in PEM fuel cells." *International Journal of Energy and Environment* 7, no. 2 (2016): 97.

[38] Atrazhev, Vadim V., Tatiana Yu Astakhova, Dmitry V. Dmitriev, Nikolay S. Erikhman, Vadim I. Sultanov, Timothy Patterson, and Sergei F. Burlatsky. "The model of stress distribution in polymer electrolyte membrane." *Journal of The Electrochemical Society* 160, no. 10 (2013): F1129. https://doi.org/10.1149/2.079310jes

[39] Ali, Karim M., Mohamed Madbouli, Hany M. Hamouda, and Amr Guaily. "A stress mapping immersed boundary method for viscous flows." *Journal of Advanced Research in Fluid Mechanics and Thermal Sciences* 87, no. 3 (2021): 1-20. https://doi.org/10.37934/arfmts.87.3.120

[40] Borkovski, Stefan, and Maja Erkechova. "Control approaches of pem fuel cells: a review." *Industry 4.0* 5, no. 3 (2020): 126-131.

[41] Costamagna, Paola, and Supramaniam Srinivasan. "Quantum jumps in the PEMFC science and technology from the 1960s to the year 2000: Part II. Engineering, technology development and application aspects." *Journal of power sources* 102, no. 1-2 (2001): 253-269. https://doi.org/10.1016/S0378-7753(01)00808-4

[42] Kandlikar, Satish G., and Zijie Lu. "Thermal management issues in a PEMFC stack–A brief review of current status." *Applied Thermal Engineering* 29, no. 7 (2009): 1276-1280. https://doi.org/10.1016/j.applthermaleng.2008.05.009

[43] Nima, Nayema Islam, and Mohammad Ferdows. "Dual solutions in mixed convection flow along non-isothermal inclined cylinder containing gyrotactic microorganism." *Journal of Advanced Research in Fluid Mechanics and Thermal Sciences* 87, no. 3 (2021): 51-63. https://doi.org/10.37934/arfmts.87.3.5163

[44] Atifi, A., H. Mounir, and A. El Marjani. "A 2D finite element model for the analysis of a PEM fuel cell heat and stress distribution." *International Review on Modeling and Simulation (IREMOS)* 8, no. 6 (2015): 632-639. https://doi.org/10.15866/iremos.v8i6.7367